Journal of Sound and Vibration 331 (2012) 1859–1869

Contents lists available at SciVerse ScienceDirect

Journal of Sound and Vibration

journal homepage: www.elsevier.com/locate/jsvi

Modeling of a passive distributed vibration control device using a superposition technique

Ryan L. Harne *, Chris R. Fuller

Vibration and Acoustics Laboratories, Department of Mechanical Engineering, Virginia Polytechnic Institute and State University, 131 Durham Hall (MC 0238), Blacksburg, VA, 24061, USA

ARTICLE INFO

Article history:
Received 5 April 2011
Received in revised form
11 December 2011
Accepted 13 December 2011
Handling Editor: S. Ilanko
Available online 27 December 2011

ABSTRACT

The modeling of a distributed vibration control device is considered for use in predicting the vibration attenuation benefits and best design practices when such devices are attached to vibrating structures. Three-dimensional (3D) finite element (FE) analysis is possible but the geometric intricacies of the distributed spring layer and potential lack of symmetries of the device placement on a host structure make such a model expensive to compute, particularly for optimization purposes. Thus, an equivalent 2D model is desirable, whereby conventional Ritz-method solution forms may be implemented. This paper describes the continuum domain model of interest and explores the applicability of a superposition approach by which a non-continuous distributed spring layer is homogenized into a 2D continuum. Simple FE models are described which allow computation of the required elasticity parameters of the spring layer. An eigenfrequency analysis comparing 3D FE and 2D model results show good agreement in the lowest order natural frequencies over a range of typical device design parameters. Experimental measurements further validate the modeling approach by comparison of FRF results. The superposition method is found to accurately model non-continuous materials such as the corrugated distributed spring layer of interest and should therefore be applicable to other embodiments of such layers.

1. Introduction

An on-going aim of passive vibration control materials is to simultaneously achieve low and high frequency structural vibration attenuation while contributing only a small additional mass to the host structure. For applications in transportation, e.g. in maritime or aerospace vehicles, the minimization of weight of the treatments and the desirability for simple, broadband passive vibration attenuation are equally important objectives. Some successful theoretical or experimental embodiments in this pursuit have featured viscoelastic, poroelastic or vertical discrete spring layers along with some form of distributed mass [1–4]. In some cases, these designs allow the passive treatment to operate in dual dynamic regimes: at low frequencies like a traditional point vibration absorber as the mass may provide a reactive forcing effect at a natural frequency; and at high frequencies in a manner identical to constraining-layer damping treatments by resistive effects.

* Corresponding author. Tel.: +1 540 231 4162.
E-mail address: rharne@vt.edu (R.L. Harne).

0022-460X/$ - see front matter © 2011 Elsevier Ltd. All rights reserved.
doi:10.1016/j.jsv.2011.12.014

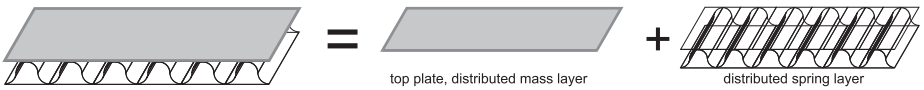

Fig. 1. The full distributed vibration control device composed of continuously distributed top mass and spring layers.

One such treatment, originally termed the distributed vibration absorber [5], utilizes a distributed corrugated spring layer and a distributed mass layer, Fig. 1. The distributed spring layer is geometrically identical to a number of common sandwich panel designs with the added feature that it is transversely compressible. While full 3D FE analysis may assist in the study of such a device when attached to an arbitrary vibrating structure, the intricacies of the device geometry and any asymmetries in the full system make solution to such a finite element model a computationally expensive task. It is therefore useful to model the coupled system in an equivalent two-dimensional, continuous domain, approximate solutions to which are much more readily achievable using approximate methods, *e.g.* the Ritz method.

However, due to the transverse deformability of the vibration control device, application of most sandwich panel theories is limited since they frequently employ incompressibility assumptions in derivation. Practically speaking, most sandwich structures are designed for *strength*, so as to avoid transverse deflection, or buckling. A few methods to include compressibility in the analysis have been explored: for example, higher-order theories (a number of which are summarily reviewed in [6]), the elastic foundation approach [7] and a superposition method [8].

The latter approach superposes incompressible sandwich panel theory with a decoupled compressible core and was found to accurately predict static and dynamic deflection and stress for sandwich panels having both symmetrical and asymmetrical geometries [9]. This method is hereby explored for the study of the distributed spring layer of the vibration control device.

Although a number of homogenization techniques for corrugated panels are available – a thorough review of available methods is described in [10] – the incompressible sandwich panel theory employed in this work follows from the derivation of Libove and Batdorf [11]. The derivation applies to sandwich panels of arbitrary, periodic cross-section and yields the bending, twisting and shear stiffnesses for an equivalent orthotropic 2D panel. This analysis also included careful laboratory experiments which may be carried out to directly calculate the approximate elasticity parameters. Cheng et al. [12] described the corresponding FE models which may substitute for the experiments and allow for quick calculation of the needed elastic constants.

The equivalent transverse stiffness for the compressible core may be approximated using classical, linear elasticity theory. Thus, the superposition of these two elastic responses may represent the full dynamic characteristics of the distributed spring layer in Fig. 1. Though the superposition approach was derived for core layers having both continuous and non-continuous contact with the facing sheets, for example both honeycomb and foam cores, its application appears to be primarily concerned with foam core, or truly continuous, materials. It does not appear that an investigation has been carried out to evaluate the applicability of this method to core layers of corrugated geometry. The determination of how useful the superposition method may be for corrugated core geometries would be beneficial for future modeling directions.

This paper aims to describe the modeling approach for the distributed vibration control device employing a circularly corrugated distributed spring layer using the superposition technique to evaluate the method's applicability to non-continuous materials. The steps by which to compute the equivalent elasticity parameters are given in detail. The continuum domain model employing these characteristics is briefly described. A numerical validation of the 2D continuum domain model is made against a 3D FE analysis by comparing computed eigenfrequencies. An apparatus for producing such circularly corrugated spring layers is described which was used to manufacture a number of metal samples for testing. Acceleration FRFs are compared between the 2D model and experimental results as final validation of the applicability of the superposition technique to non-continuous materials.

2. Modeling methodology

The geometry desired to study is shown in Fig. 2. A vibration control device having a distributed, woven spring layer is attached to a base plate having both arbitrary boundary conditions as well as arbitrary excitation. The vibration control device is composed of two components: a top plate, representing the distributed mass layer, and a transversely flexible, anisotropic spring layer, Fig. 1. The spring layer itself is constructed from a periodic, corrugated core sheet bounded by two thin facing sheets, similar to many conventional sandwich panel designs.

The vibration control device with a distributed spring layer having a woven core exhibits dynamic behavior ascribed to both conventional single degree-of-freedom (SDOF) vibration absorbers and constrained layer damping treatments, Fig. 3(a) and (b), respectively. In addition, the core layer uses a sandwich design having apparent anisotropic stiffnesses. Therefore, a continuum domain model suitable to assess vibration control devices using such a distributed spring layer requires the combination of equivalent anisotropic material properties as well as flexible core characteristics.

In the proposed model, the sandwich structure is considered to be a superposition of an incompressible, orthotropic thick plate and a compressible core of vertical spring elements, Fig. 4. The latter springs are allowed to deflect only in the transverse direction and have no coupling to the incompressible plate response.

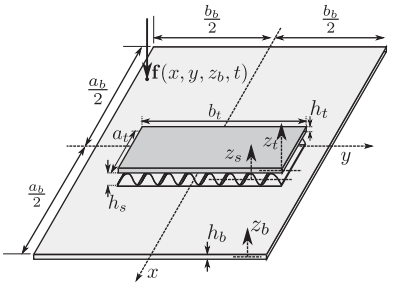

Fig. 2. Vibration control device attached to an arbitrarily bounded base plate excited by a point force (subscripts *b*,*s*,*t* indicate base, spring layer and top plates, respectively). Transverse axes, *z*, are defined from the undeformed middle-plane of their respective layer.

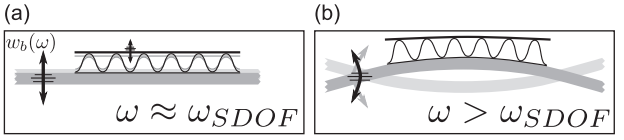

Fig. 3. Device response to host structural vibration (a) close to and (b) above the device SDOF natural frequency. Around the natural frequency, the device operates like a mass–spring oscillator, while above the frequency the device resists structural motion like constraining treatments.

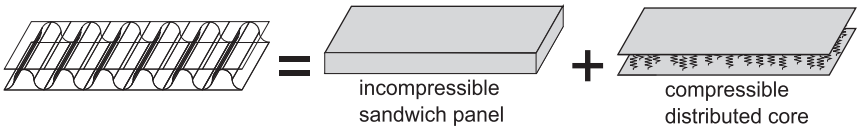

Fig. 4. Approximation of compressible spring layer as the superposition of an incompressible core with a layer of transversely compressible springs.

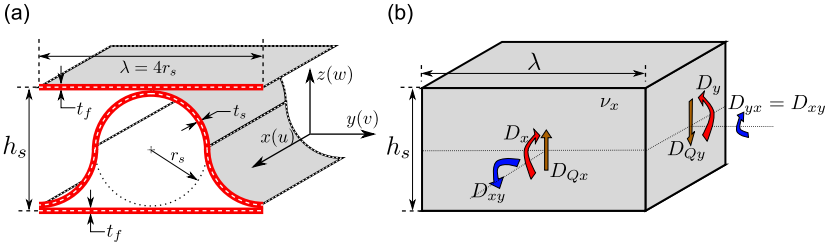

Fig. 5. Periodic geometry of an (a) unit depth circular core sandwich panel transformed into (b) an equivalent, continuous orthotropic thick plate.

2.1. Equivalent incompressible core elastic properties calculations

Libove and Batdorf [11] derived a theory for the determination of equivalent orthotropic plate properties for incompressible sandwich panels having an arbitrary core design, thereby transforming the exact core geometry into an equivalent, symmetric and continuous 2D domain, Fig. 5, having equivalent bending and shearing stiffnesses D_x, D_y, D_{Qy}, D_{Qx} and D_{xy}. Included with the derivation were a series of laboratory tests which may be carried out to determine the elasticity constants. Cheng et al. [12] then proposed and validated a set of corresponding FE models to expedite the computation of such elastic properties. The latter FE models are here employed for the present sandwich structure having period (or wavelength) λ, facing sheet thickness t_f and corrugated sheet thickness t_s.

The distortion equations for the incompressible sandwich panel are [11]

$$\kappa_x = \frac{\partial^2 w}{\partial x^2} = -\frac{M_x}{D_x} + \frac{\nu_y M_y}{D_y} + \frac{1}{D_{Qx}}\frac{\partial Q_x}{\partial x} \tag{1}$$

$$\kappa_y = \frac{\partial^2 w}{\partial y^2} = -\frac{M_y}{D_y} + \frac{\nu_x M_x}{D_x} + \frac{1}{D_{Qy}}\frac{\partial Q_y}{\partial y} \tag{2}$$

$$\kappa_{xy} = \frac{\partial^2 w}{\partial x \partial y} = \frac{M_{xy}}{D_{xy}} + \frac{1}{2}\frac{1}{D_{Qx}}\frac{\partial Q_x}{\partial y} + \frac{1}{2}\frac{1}{D_{Qy}}\frac{\partial Q_y}{\partial x} \tag{3}$$

$$\gamma_{yz} = \frac{Q_y}{D_{Qy}} \tag{4}$$

$$\gamma_{xz} = \frac{Q_x}{D_{Qx}} \tag{5}$$

where M_x and M_y are internal bending moments, M_{xy} is the internal twisting moment, Q_x and Q_y are internal shearing forces, and v_x and v_y are the Poisson's ratios coupling the bending responses. These moments and forces are labeled for a unit core cross-section in Fig. 5(b) having thickness h_s and period length λ. The curvatures and twist, κ_x, κ_y and κ_{xy}, are defined about the middle-plane of the panel and γ_{yz} and γ_{xz} are the transverse shear strains.

The facing sheets and the core layer are considered to be isotropic materials. The FE models to calculate the equivalent stiffnesses for the sandwich structure define a 3D geometry of a certain section of the sandwich core, apply the loads described in the distortion equations and calculate the resulting strains or displacements from key nodes. Shell elements are employed for each model.

The FE models to compute the elastic constants of the incompressible sandwich panel – E_x, E_y, G_{xy}, G_{yz}, G_{xz} and v_x – are depicted in Fig. 6. The models to compute E_x and G_{xz} use geometries of a single core period with a length of sufficient span so as to ignore end effects. Increasing this length naturally reduces the influence of potential end effects on the center of the specimen, but is more costly to compute due to the increased number of elements. The models to calculate E_y and G_{yz} use multiple periods of the sandwich structure and a depth equal to or greater than the period length. The model to calculate twisting stiffness, G_{xy}, uses a geometry of equal length and depth.

Unit moments per area are applied to rigid end elements in the models to compute bending stiffnesses. Rigid elements are modeled by using a Young's modulus six orders of magnitude greater than the facing sheet value. For the twisting stiffness model, unit moments are applied without rigid end planes, since additional rigidity would inhibit the sample deflection. Unit forces per length are applied to the rigid end elements of the models to compute shearing stiffnesses. The latter two models, Fig. 6(d) and (e), include fixed points, P_f, on the bottom facing sheets in order to prevent rigid body motion of the sandwich core. In each model, sides of the geometry to which no moments or forces are applied are given boundary conditions of symmetry. This implies that displacements in the co-ordinate axis normal to the plane of symmetry must be zero.

In Fig. 6, the desired outputs of each model are provided in inset boxes. Bending and shearing strains are output at centrally-positioned nodes on the top and bottom facing sheets for the models to compute bending and twisting stiffnesses, respectively. Displacements of the facing sheets from the undeformed configurations are output from the models to compute shearing stiffnesses. In Fig. 6(e), the transverse deflection, δz, is output from a node spaced Δx away from the centrally-located fixed point, P_f.

Using the strains or displacements the bending and twisting curvatures or shearing strains are calculated as follows [12]:

$$\kappa_x = \frac{\epsilon_{x1} - \epsilon_{x2}}{h_s}, \quad \kappa_y = \frac{\epsilon_{y1} - \epsilon_{y2}}{h_s}, \quad \kappa_{xy} = \frac{\gamma_{xy1} - \gamma_{xy2}}{2h_s} \tag{6}$$

$$\gamma_{yz} = \frac{\delta y}{h_s} + \frac{2\delta z}{\lambda}, \quad \gamma_{xz} = \frac{\delta x}{h_s} + \frac{\delta z}{\Delta x} \tag{7}$$

These parameters are related to the bending and shear stiffnesses by

$$D_x = -\frac{M_x}{\kappa_x}, \quad D_y = -\frac{M_y}{\kappa_y}, \tag{8}$$

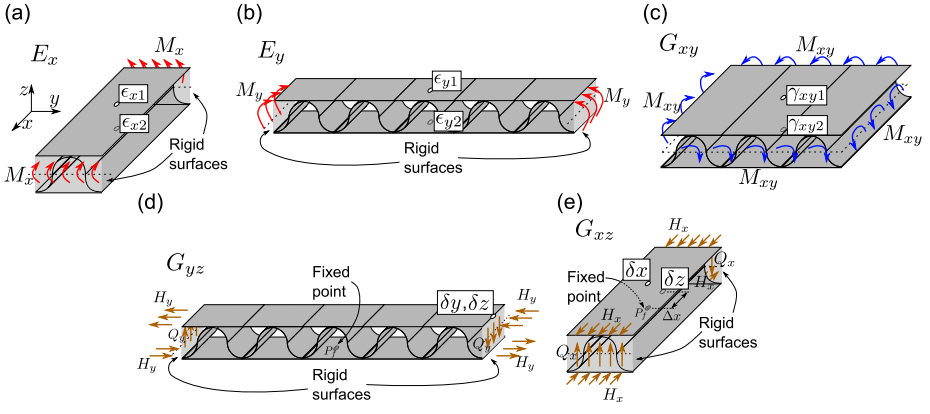

Fig. 6. FE models for computation of (a) E_x, (b) E_y, (c) G_{xy}, (d) G_{yz} and (e) G_{xz}.

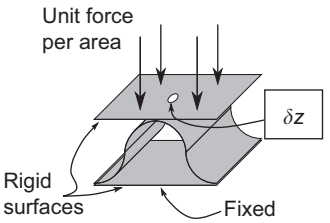

Fig. 7. FE model to compute the transverse elastic constant, E_z.

$$\nu_x = \frac{\kappa_y}{M_x/D_x}; \quad \frac{\nu_x}{D_x} = \frac{\nu_y}{D_y} \tag{9}$$

$$D_{xy} = \frac{M_{xy}}{\kappa_{xy}}, \quad D_{Qy} = \frac{Q_y}{\gamma_{yz}}, \quad D_{Qx} = \frac{Q_x}{\gamma_{xz}} \tag{10}$$

Presently, unit moments per area and unit shear forces were employed in the FE models, and thus Eqs. (8) and (10) are straightforward to calculate.

From the computed stiffnesses may be found the equivalent elastic material properties representing a 2D incompressible, symmetrical orthotropic plate

$$E_x = \frac{12D_x}{h_s^3}, \quad E_y = \frac{12D_y}{h_s^3} \tag{11}$$

$$G_{xy} = \frac{6D_{xy}}{h_s^3}, \quad G_{yz} = \frac{D_{Qy}}{k_s h_s}, \quad G_{xz} = \frac{D_{Qx}}{k_s h_s} \tag{12}$$

$$\nu_{xy} = \nu_x, \quad \nu_{yx} = \nu_y \tag{13}$$

where the shear factor is $k_s = 5/6$. Finally, the equivalent density of the anisotropic plate is calculated as the product of the core sheet material density, ρ, multiplied by the ratio of the actual material volume to the volume of the equivalent continuous element. For the circular cross-section, this may be computed as

$$\rho_s = \rho \frac{\pi t_s}{\lambda} \tag{14}$$

2.2. Equivalent transverse elastic property calculation

To compute the equivalent transverse elastic constant, E_z, representing the distribution of vertical spring elements of the sandwich core layer, Fig. 4, requires one additional FE model. Fig. 7 depicts the model geometry, loading conditions and model output. Since the facing sheets of the sandwich structure do not carry any of the transverse loading in the actual distributed spring layer (recall that the layer is ultimately bounded by a base plate and a top plate), the facing sheets are modeled using rigid elements. A unit force per area is applied to the top facing sheet while the bottom sheet is kept fixed. The boundary planes on each of the four section faces are symmetric as in the earlier FE models; this restricts the sandwich structure to transverse deflection only. The desired output of the model is the transverse deflection of a node of the top facing sheet, δz.

The equivalent transverse elastic parameter may then be computed as

$$E_z = \frac{Fh_s}{\delta z} \tag{15}$$

where F is the force per area applied to the top surface.

3. Continuum domain model

3.1. Generalized Hamilton's principle for the coupled system

For the sake of conciseness and to focus more on the numerical implementation, a brief description of the mathematical formulation of the model is presented. The variational method used in the model is based on the generalized Hamilton's principle for deformable mechanical bodies [13]

$$\delta \int_{t_1}^{t_2} [(T-U)+\overline{W}]\, \mathrm{d}t = 0 \tag{16}$$

where T is the total kinetic energy, U is the total strain energy and $\overline{W}$ are the mechanically applied loads. For each individual layer, these components are calculated from

$$U_i = \frac{1}{2}\int_{V_i} (\mathbf{S}^T\mathbf{T})_i \, dV_i, \quad K_i = \frac{1}{2}\rho_i \int_{V_i} [\dot{u}^2 + \dot{v}^2 + \dot{w}^2]_i \, dV_i \tag{17}$$

$$\overline{W}_i = \sum_{j=1}^{N_f} [u(x_j)v(y_j)w(z_j)]_i \cdot [f_x f_y f_z]_j^T$$

where the subscript $i = b,s,t$ represents the layering convention indicated in Fig. 2, $\mathbf{S}$ and $\mathbf{T}$ are the appropriate strain and stress tensors for the layer, respectively, f represents applied point loads, N_f are the number of applied loads and T is the transpose operator.

The base plate and the top plate are modeled with Love–Kirchhoff assumptions. Thus, the displacement expressions are written in terms of linear Taylor series expansions about the mid-plane displacements. The displacement expressions for the distributed spring layer are linear expansions in the cross-planar co-ordinates and a quadratic Taylor series expansion for the flexural component

$$u(x,y,z,t)_s = u_o(x,y,t) + z_s\theta_y(x,y,t) \tag{18}$$

$$v(x,y,z,t)_s = v_o(x,y,t) + z_s\theta_x(x,y,t)$$

$$w(x,y,z,t)_s = w_o(x,y,t) + z_s\frac{\partial w_o}{\partial z_s} + \frac{1}{2}z_s^2\frac{\partial^2 w_o}{\partial z_s^2}$$

where the subscript o indicates the middle plane of the layer. The orthotropic constitutive relation for the distributed spring layer is expressed as

$$\begin{bmatrix}\sigma_{xx}\\ \sigma_{yy}\\ \sigma_{zz}\\ \tau_{yz}\\ \tau_{xz}\\ \tau_{xy}\end{bmatrix}_s = \begin{bmatrix} \frac{E_x}{1-\nu_{xy}\nu_{yx}} & \frac{\nu_{yx}E_x}{1-\nu_{xy}\nu_{yx}} & 0 & 0 & 0 & 0 \\ \frac{\nu_{xy}E_y}{1-\nu_{xy}\nu_{yx}} & \frac{E_y}{1-\nu_{xy}\nu_{yx}} & 0 & 0 & 0 & 0 \\ 0 & 0 & E_z & 0 & 0 & 0 \\ 0 & 0 & 0 & G_{yz} & 0 & 0 \\ 0 & 0 & 0 & 0 & G_{xz} & 0 \\ 0 & 0 & 0 & 0 & 0 & G_{xy} \end{bmatrix}_s \begin{bmatrix}\epsilon_{xx}\\ \epsilon_{yy}\\ \epsilon_{zz}\\ \gamma_{yz}\\ \gamma_{xz}\\ \gamma_{xy}\end{bmatrix}_s \tag{19}$$

Eq. (19) indicates the decoupled nature of the anisotropic sandwich panel dynamics with those of the transversely flexible core. Damping is included in the study by means of an isotropic loss factor, η_i, for each of the three layers in the system.

Continuity of displacements, transverse normal and transverse shearing stresses are applied at the interfaces between the distributed spring layer and the bounding base and top plates. This allows the full system response to be described in terms of the mid-plane displacement components of the base and top plates: $[u_o(x,y,t)\ v_o(x,y,t)\ w_o(x,y,t)]_b$ and $[u_o(x,y,t)\ v_o(x,y,t)\ w_o(x,y,t)]_t$, respectively.

3.2. Rayleigh–Ritz solution

To approximate the dynamic response of the system, the Rayleigh–Ritz method is employed for the 6 unknowns. The Rayleigh–Ritz approximate solutions may be expressed as

$$(u_o)_t(x,y,t) = \Lambda(x,y)\mathbf{f}(t), \quad (v_o)_t(x,y,t) = \Pi(x,y)\mathbf{g}(t), \quad (w_o)_t(x,y,t) = \Gamma(x,y)\mathbf{h}(t)$$

$$(u_o)_b(x,y,t) = \Phi(x,y)\mathbf{p}(t), \quad (v_o)_b(x,y,t) = \Theta(x,y)\mathbf{r}(t), \quad (w_o)_b(x,y,t) = \Psi(x,y)\mathbf{s}(t) \tag{20}$$

where Λ, Π, Γ, Φ, Θ and Ψ are the admissible trial function sets used in the linear combination, each multiplied by a vector of generalized co-ordinates. The hierarchical trigonometric function set of Beslin and Nicolas [14] is employed as the trial function series since it is convenient for simulation of the classical boundary conditions of plates: simply-supported, clamped and free suspension. Substituting this form of approximate solution into Eq. (16) and assuming an harmonic time dependence yields

$$[-\omega^2(\mathbf{M_t}+\mathbf{M_s}+\mathbf{M_b}) + (\mathbf{K_t}+\mathbf{K_s}+\mathbf{K_b})]\mathbf{m} = \mathbf{B_f}\mathbf{f} \tag{21}$$

with

$$\mathbf{m} = [\mathbf{f}\ \mathbf{g}\ \mathbf{h}\ \mathbf{p}\ \mathbf{r}\ \mathbf{s}]^T \tag{22}$$

The matrices to the left-hand side of Eq. (21) represent the mass, $\mathbf{M}$, and stiffness, $\mathbf{K}$, matrices of the three layers, evaluated using the six assumed solutions, Eq. (20). The matrices resulting from the distributed spring layer, denoted by subscript s,

fully couple the extensional and flexural displacements of the top and base plates. Finally, $\mathbf{B_f}$ are the basis functions evaluated at the location of the applied forces, $\mathbf{f}$.

In the absence of any forcing, an eigenvalue problem is solved yielding the natural frequencies of the coupled system

$$[\mathbf{K_t}+\mathbf{K_s}+\mathbf{K_b}]\mathbf{m}=\omega^2[\mathbf{M_t}+\mathbf{M_s}+\mathbf{M_b}]\mathbf{m} \tag{23}$$

4. Numerical validation: eigenfrequency analysis

The continuum domain model and superposition technique are evaluated by calculating the eigenfrequencies of a sample vibration control device. The isotropic properties of the base plate, the top plate, facing sheets and core sheet are provided in Table 1. The above FE models were employed and the computed equivalent elastic parameters of the sandwich spring layers are presented in Table 2.

It was assumed that the facing sheets of the spring layer are of equal thickness to the core sheet, *i.e.* $t_f=t_s$. Though it may be the case in practice that the corrugated spring layer could itself be attached to the top mass layer and base plate, there are a number of manufacturing processes presently available which necessitate the use of the facing sheets to maintain the shape of the corrugation during construction, *e.g.* extrusion manufacture. It is here assumed that the facing and core sheet thicknesses and material compositions are equal. In each case, the thickness of the equivalent spring layer was $h_s=6.35$ mm with a periodic length of $\lambda=12.7$ mm.

The base plate of the system is considered to be fixed over the full surface. This would represent the case of the vibration control device being attached to a completely rigid surface. A full 3D FE model of the system was constructed using the exact geometry and isotropic material properties of the facing and core sheets, Table 1, with loss factors extracted from [15]. Both the 3D FE and the 2D continuum domain models were evaluated for the first 4 eigenfrequencies and mode shapes of the coupled system and the results are presented in Table 3. Percentage differences are provided for the 2D domain models, with reference to the 3D FE solutions.

The first four mode shape dynamics, as output from the 2D domain model, are illustrated in Fig. 8. The first, second and third mode shapes exhibit rigid body motion of the device top mass layer: the first mode is back-and-forth rocking of the mass; the second mode shape is rigid body rotation of the mass about the x-axis; the third mode shape is rigid body rotation of the mass about the y-axis. Interestingly, the SDOF oscillation of the top mass layer, that which yields the traditional vibration absorber (reactive) behavior of the device, does not occur until the fourth mode.

From Table 3 it is observed that the SDOF natural frequency occurs at almost the same frequency as those for rigid body rotations of the mass layer. The rocking mode shape, however, occurs at a lower frequency, sometimes as much as 30%

Table 1
Isotropic properties of base, top and spring layer plates, $i=b,t,s$, and the facing and core sheets.

Layer	a_i m	b_i m	h_i (mm)	E_i Pa	ν_i	ρ_i (kg/m^3)	η_i
Base	0.15	0.15	2	2.1e11	0.33	7850	3e−4
Top	0.102	0.102	2	2.1e11	0.33	7850	3e−4
Equivalent 2D spring layer	0.102	0.102	6.35	n/a	n/a	n/a	5e−3
Facing/core sheets	n/a	n/a	n/a	2.1e11	0.33	7850	3e−4

Table 2
Equivalent orthotropic plate properties of spring layers.

t_s (μm)	E_x (Pa)	E_y (Pa)	E_z (Pa)	ν_{xy}	G_{yz} (Pa)	G_{xz} (Pa)	G_{xy} (Pa)	ρ_s (kg/m^3)
50.8	2.329e12	2.031e12	1.147e6	0.0913	8.186e6	2.614e8	7.608e9	98.65
76.2	3.451e12	2.996e12	3.695e6	0.0877	1.526e7	2.042e8	9.836e9	148.0

Table 3
Natural frequencies (Hz) as computed by 3D FE analysis and 2D model (percent difference).

t_s (μm)	Model	Mode 1	Mode 2	Mode 3	Mode 4
50.8	3D FE	362.8	536.8	538.5	540.4
	2D	360.0 (−0.7%)	529.6 (−1.3%)	530.3 (−1.5%)	536.3 (−0.7%)
76.2	3D FE	652.7	957.7	960.4	964.1
	2D	644.7 (−1.2%)	937.9 (−2.1%)	939.7 (−2.1%)	957.5 (−0.6%)

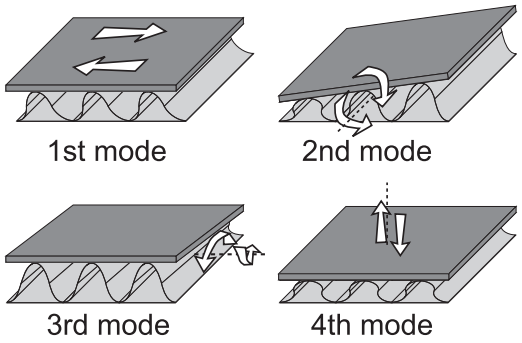

Fig. 8. First four mode shapes of device having a fixed based.

lower in frequency than the rotational oscillations. This dynamic is caused by the relatively small shearing stiffness, G_{yz}, a feature which such corrugated sandwich panel designs are known to exhibit.

Table 3 shows that the 2D continuum domain model yields natural frequencies in close agreement with the full 3D FE model. Though the SDOF natural frequency of the device is the fourth eigenmode, this is still anticipated to be the dominant response of the full vibration absorber device in practice. Since structural motion at low frequencies is primarily modal and flexural, the attached devices are likely to be excited with mostly transverse structural motion, as in Fig. 3(a). Though there are several rigid body rotations of the device found to exist close in frequency to this SDOF response, the devices are primarily excited by transverse oscillation and, as such, only the fourth eigenmode is likely to be observed in practice.

5. Experimental validation: FRF comparison

5.1. Spring layer construction description

Circularly corrugated materials are commonly available in two principal forms: as corrugated cardboard or as corrugated plastic layers. Both are also produced using sinusoidal corrugations. However, after adding a mass layer to these corrugated materials, in both instances the equivalent transverse stiffness is too great to yield a SDOF natural frequency in the bandwidth of interest, $<$ 500 Hz. Thus, a new manner was sought to manufacture a circularly corrugated spring layer, particularly one using metal materials.

A spot welding device was manufactured especially designed for this purpose. The corrugated layer was first woven through adjacent, constrained copper tubes until the full length of the spring layer was held in form. Then, a facing sheet was applied to the top side. The spot welder was connected to a desired copper tube and the welding arm was brought down upon the facing sheet. This generated an appropriate point weld at the connection of the corrugated layer and the facing sheet. With extensive practice, this method was refined so as to yield both extremely consistent circularly corrugated shapes as well as minimal heat affected zones.

Fig. 9 shows one such corrugated layer, next to a quarter piece for scale, produced to specifically show the advancement of this process. The thickness of the steel facing and core sheets were $t_f = t_s = 50.8$ μm having a $\lambda = 12.7$ mm. Thicker layers, *e.g.* larger λ, were produced with greater ease and the thinnest facing/core sheet material observed to be weld-able by this method was approximately $t_f = t_s = 25$ μm. It was not always necessary to weld both facing sheets to the corrugated layer and, on some occasions, the mass layer was directly welded to the spring layer to yield the full vibration control device.

5.2. FRF test results and comparison

A number of the spot-welded vibration control devices were carefully produced using the same circularly corrugated wavelength, $\lambda = 44.4$ mm, but increasing thicknesses of the corrugated steel material, $t_s = 25.4$, 50.8 and 76.2 μm. The anticipated result of this change was to yield steadily higher SDOF natural frequencies with each increase in corrugated material thickness. The devices were attached to a stiff shaker table exciting them equally at all frequencies with transverse vibration, Fig. 10. Accelerometers were attached to the top center of the mass layer and one to the shaker platform itself. The FRF between the accelerations was anticipated to primarily observe the SDOF resonance, the fourth eigenmode from Section 4, since excitation was assumed to be strictly one-dimensional transverse vibration.

To model the FRF of the devices, the stiff base plate was described using the properties given in Table 4. The base plate was considered to have free boundary conditions and excited by a centrally located, transverse point force: $f_z = 1$ N. The attached vibration control devices were centered on the base plate. The top plate properties, remaining the same for each of the three spring layers used, are given in Table 4. The computed equivalent elasticity parameters for each of the three spring layers are provided in Table 5 which employed the steel facing and core sheet materials just as manufactured.

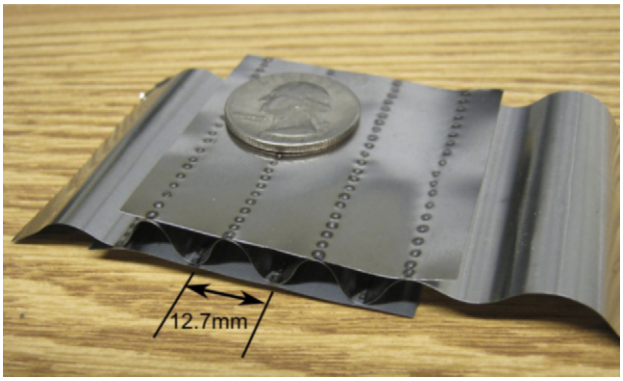

Fig. 9. Photograph of sample spot-welded circularly corrugated spring layer ($\lambda = 12.7$ mm and $t_s = t_f = 50.8$ μm) manufactured after refinement of construction procedure.

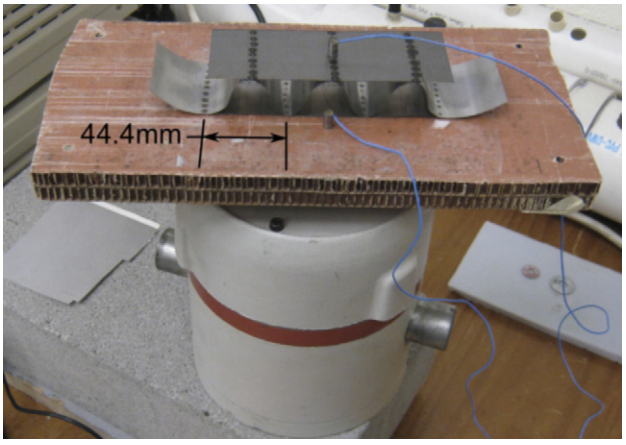

Fig. 10. Device attached to rigid shaker platform for FRF testing. The top mass layer of this device is shown to be directly attached to the corrugated layer without the presence of the additional facing sheet.

Table 4
Isotropic properties of base and top plates, $i = b,t$, and the facing and core sheets.

Layer	a_i (m)	b_i (m)	h_i (mm)	E_i (Pa)	ν_i	ρ_i (kg/m^3)	η_i
Base	0.355	0.152	10	1e13	0.33	800	3e−4
Top	0.133	0.0508	0.454	2.1e11	0.33	6044	3e−4
Facing/core sheets	n/a	n/a	n/a	2.1e11	0.33	7850	3e−4

Table 5
Equivalent orthotropic plate properties of spring layers.

t_s (μm)	E_x (Pa)	E_y (Pa)	E_z (Pa)	ν_{xy}	G_{yz} (Pa)	G_{xz} (Pa)	G_{xy} (Pa)
25.4	1.014e11	9.112e10	1.164e4	0.07739	7.948e5	4.909e6	1.625e9
50.8	1.979e11	1.742e11	4.593e4	0.08455	1.706e6	1.856e7	5.267e9
76.2	2.939e11	2.572e11	1.205e5	0.09105	2.744e6	5.401e7	7.550e9

The FRF response was calculated as the ratio of the out-of-plane acceleration of the top plate to the acceleration of the base plate:

$$\mathrm{FRF}(\omega) = 20\log_{10}\left[\frac{(w_o)_t(x_1,y_1,\omega)}{(w_o)_b(x_2,y_2,\omega)}\right] \tag{24}$$

where $(x_1,y_1) = (0,0)$ and $(x_2,y_2) = (0,0)$, the normalized centers of the plates.

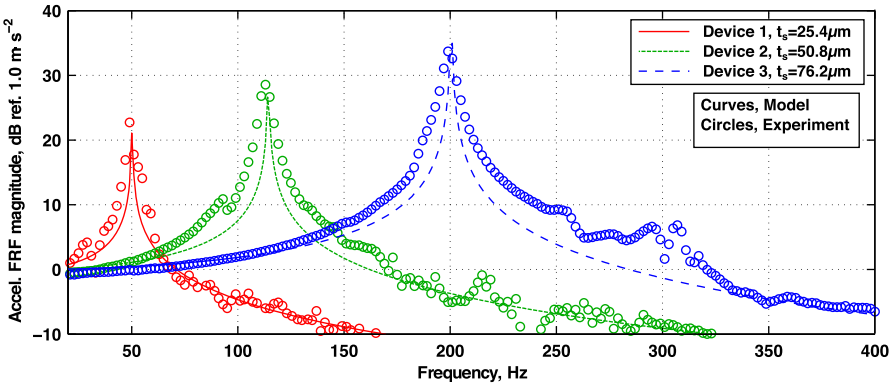

Fig. 11. Comparison of measured (circles) and modeled (solid curves) FRF responses for device having $t_s = 25.4$ μm (red plot), $t_s = 50.8$ μm (green plot) and $t_s = 76.2$ μm (blue plot). (For interpretation of the references to color in this figure legend, the reader is referred to the web version of this article.)

Fig. 11 plots the comparison of modeled and measured FRF response of the three vibration control devices. As anticipated, only the SDOF natural frequency, or the fourth eigenmode, is excited by this test, typical of one-dimensional mass–spring systems. The model exactly predicts the location of the SDOF resonance for each device. As expected, the use of thicker materials in the spring layer increases the SDOF natural frequencies. However, one feature of this which the model does not fully reproduce is the corresponding increase in damping as the corrugated material thickness increases.

It is observed for $t_s = 50.8$ μm and $t_s = 76.2$ μm that the model underpredicts the level of damping in the spring layer around resonance. This additional damping may be explained by the use of an isotropic loss factor damping model which is proportional to stiffness and not to mass. The mass of each successive spring layer increases by two and three times the first sample which used a corrugated thickness of $t_s = 25.4$ μm. Where a more generalized Rayleigh damping model used, the additional mass-proportional weighting may help account for the observed damping increase. The determination of both mass- and stiffness-proportional terms may thereafter require trial and error estimation as compared with the experimental results.

6. Conclusions

In this paper, a continuum domain model of a distributed vibration control device was proposed which has the advantage of reduced computational expense as compared with full 3D FE analysis. Crucial to the model is the homogenization of a distributed spring layer into the superposition of an incompressible sandwich panel and a compressible core. The methods to employ this approach and its validity as compared with 3D FE analysis and experimental results were explored.

The continuum domain model was found to be in very close agreement in an eigenfrequency analysis with 3D FE models of vibration control device designs employing circular corrugations in the spring layer. Most evident are dynamics of the device which are not otherwise observed for one-dimensional, mass–spring–damper systems, indicating that the device is capable of also suppressing structural motion through constraining-type effects as the spring layer extensionally deforms. The ability to both reactively work against and resistively suppress structural motion suggests that the distributed vibration control devices should be useful over a broader range of frequencies than either point oscillators or constraining treatments alone.

Several experimental samples were manufactured using a spot welding device constructed especially for the purpose of manufacturing the circularly corrugated spring layers using very thin steel materials. The samples were attached to a shaker platform and acceleration FRF measurements were compared against the modeled results. The location of the SDOF resonances were in exact agreement between measurement and model. However, the model is found to underpredict the magnitude of damping observed as the thickness of the corrugated material increased. This could be due to the basic loss factor (stiffness-proportional) damping model which does not take into account mass effects. The more generalized Rayleigh damping model may correct this deficiency.

The superposition technique is found to accurately represent the dynamics of non-continuous materials, namely the circularly corrugated structure under study. Thus, more computationally efficient 2D modeling of such distributed vibration control devices employing other non-continuous layers as distributed springs may be employed for estimation of their benefit upon host vibrating structures.

In practice, to yield a SDOF natural frequency in the typical range flexural structural vibration, $<$ 500 Hz, the thicknesses of the corrugated material must be very thin. This makes manufacture of the distributed spring layer difficult and subject to novel construction methods since controlled extrusion processes are not often possible in this regime of material thickness. Nevertheless, the possibility to construct a continuously distributed vibration control device capable of both resistive and reactive effects on a host structure encourages innovative solutions to this problem.

Acknowledgments

The authors are grateful for the continued support of Newport News Shipbuilding and technical monitor Kevin Smith. The authors would also like to recognize the invaluable assistance of Dr. Cory Papenfuss in the design and construction of the spot welding rig.

References

[1] J.A. Zapfe, G.A. Lesieutre, Broadband vibration damping using highly distributed tuned mass absorbers, *AIAA Journal* 35 (4) (1997) 753–755.
[2] Y. Liu, K.W. Wang, Enhanced active constrained layer damping treatment for broadband vibration suppression, *Journal of Vibration and Control* 8 (6) (2002) 777–803.
[3] S.J. Estéve, M.E. Johnson, Reduction of sound transmission into a circular cylindrical shell using distributed vibration absorbers and Helmholtz resonators, *Journal of the Acoustical Society of America* 112 (6) (2002) 2840–2848.
[4] D.J. Thompson, A continuous damped vibration absorber to reduce broad-band wave propagation in beams, *Journal of Sound and Vibration* 311 (3–5) (2008) 824–842.
[5] C.R. Fuller, P. Cambou, An active–passive distributed vibration absorber for vibration and sound radiation control, *Journal of the Acoustical Society of America* 104 (3) (1998) 1851.
[6] J.N. Reddy, On refined computational models of composite laminates, *International Journal for Numerical Methods in Engineering* 27 (2) (1989) 361–382.
[7] O.T. Thomsen, Theoretical and experimental investigation of local bending effects in sandwich plates, *Composite Structures* 30 (1) (1995) 85–101.
[8] Y. Frostig, M. Baruch, Bending of sandwich beams with transversely flexible core, *AIAA Journal* 28 (3) (1990) 523–531.
[9] Y. Frostig, Classical and high-order computational models in the analysis of modern sandwich panels, *Composites: Part B* 34 (2003) 83–100.
[10] A.K. Noor, W.S. Burton, Computational models for sandwich panels and shells, *Applied Mechanics Reviews* 49 (3) (1996) 155–199.
[11] C. Libove, S.B. Batdorf, A general small-deflection theory for flat sandwich plates, *National Aeronautics and Space Administration Report No. 899*1948, pp. 139–156.
[12] Q.H. Cheng, H.P. Lee, C. Lu, A numerical analysis approach for evaluating elastic constants of sandwich structures with various cores, *Composite Structures* 74 (2006) 226–236.
[13] L. Meirovitch, *Analytical Methods in Vibrations*, Macmillan, University of Michigan, 1967.
[14] O. Beslin, J. Nicolas, A hierarchical functions set for predicting very high order plate bending modes with any boundary conditions, *Journal of Sound and Vibration* 202 (5) (1997) 633–655.
[15] L. Cremer, M. Heckl, B.A.T. Petersson, *Structure-Borne Sound: Structural Vibrations and Sound Radiation at Audio Frequencies*, third ed., Springer, Berlin, 2005.